A Knowledge-based approach to urban land use classification using AVIRIS imagery and LiDAR data

Prarthna Dhingra[1], Asfa Siddiqui[2], Vinay Kumar[2], Prabhashini Mohapatra[3], K. Venkata Reddy[1]
[1]*Department of Civil Engineering, National Institute of Technology, Warangal, Telangana, India*
[2]*Indian institute of Remote sensing, Dehradun, Uttrakhand, India*
[3]*National institute of Technology, Karnataka, India*
Emails: prarthna.dhingra@gmail.com, asfa@iirs.gov.in, vinaykumar@iirs.gov.in, prabhashini10@gmail.com, kvreddy@nitw.ac.in

***Abstract* - In this paper, the joint effect of hyperspectral and light detection and ranging (LiDAR) data for urban land use/ land cover (LULC) classification has been analyzed as combination of two data sources can result in better classification as compared to single data source. LULC classification of urban areas is a difficult task due to high spectral and spatial variability, especially with the use of single data source. The result of spectral angle mapper (SAM) classification, a supervised classification method, on hyperspectral imagery is compared with that of a knowledge based classification (KBC) combining LiDAR and hyperspectral data. Spectra from ASTER library was used as reference spectra for SAM classification while for Knowledge based classification nDSM derived from LiDAR data and indices derived from Hyperspectral data has been used. It was found that knowledge based classification had 7-8% more accuracy than SAM classification. Thus, it can be concluded that Knowledge based classification can be used as an efficient technique in this area.**

Index Terms – Knowledge-based classification, Hyperspectral, Normalized Digital surface model (nDSM)

I. INTRODUCTION

Over the time, many studies have investigated the use of remote sensing technology in urban land-use classification. Although, most analysis in urban areas is being done using aerial photography as a data source. Recent advances in space borne systems, provide alternatives to aerial photography, and implemented the use of multispectral imagery, Hyperspectral images as well as LiDAR derived data images.

However, use of remote sensing in accurate land use classification has always been a difficult task. There are several reasons for this difficulty: (*i*) It is difficult to classify manmade urban structure due to their spectral heterogeneity at small scales [1] [2] [3]. (*ii*) The complexity of urban areas makes it difficult for a single remote sensing source to meet all the requirements of precise classification [4] [5] [1]. (*iii*)Most pixels in urban areas appear to be mixed at low spatial resolution which prevents accurate land use classification [6].

The development of hyperspectral sensors has improved the accuracy of discrimination between similar land use classes as they provide hundreds of narrow continuous spectral bands from visible to shortwave infrared parts of electromagnetic spectrum [7]. Due to its advantages hyperspectral remote sensing has been increasingly used in various applications including land use classification [8]. However, due to spectral complexity in urban areas, even hyperspectral images alone are not enough for classification [9] [10]; accurate classification of urban areas requires multi source remote sensing images.

Unlike other remote sensing data, LiDAR has the advantage of providing a third dimension of height which can be used to separate classes of different heights such as buildings and roads in urban areas [11] [12]. The elevation information of the LiDAR data is very helpful in separating similar spectral signatures when it is used in combination with hyperspectral data [11]. Debes, et al., 2013 [28] investigated how the fusion of hyperspectral and LiDAR data provides improvements over traditional automated methods such as feature extraction and supervised pixel based classification. Huang, et al., 2008 [30] performed a traditional pixel level classification using multispectral and LidAR data and to further improve the accuracy they proposed a knowledge based classification system that included a rule based scheme and a knowledge based correction.

In this study we evaluate improvements in classification by integrating airborne Hyperspectral (AVIRIS data) and LiDAR data for classifying different urban land features. The main objectives of this study are to explore: (*i*) The performance of combined LiDAR and Hyperspectral data for urban land-use classification, especially the contribution of LiDAR height information for land-use classification in the areas of similar spectral signature (*ii*) The efficiency of knowledge based classification by specifying a set of rules for establishing a decision based system by defining an integrative decision tree including three dimensional information data bases and two spectral indices. The goal is to derive an efficient classified image using both the spectral information of Hyperspectral data and the spatial information of LiDAR data.

II. Study Area and Data sets

A. Study site

The study area selected is a south central part of the city of San Diego (Latitude 32o 41', Longitude -117o 6') in the state of California, USA shown in figure 1. The region lies on the coast of the Pacific Ocean in Southern California, on an average elevation of 25m above the mean sea level with an area of about 4.2 km^2.

Land use classification in this particular area is challenging because of the following issues: (*i*) spectral similarity between roads and highway leads to misclassification (*ii*) the mixed pixels [6] (*iii*) spectral similarity between rooftops and roads (*iv*) most buildings are surrounded by trees which leads to difficulty in identifying building footprints.

B. *Data*

1) LiDAR data: Lidar data has been downloaded from Data/Open Topography where it is freely available, URL: http://opentopo.sdsc.edu/lidar. This airborne data was acquired during the survey done between 03/16/2005 - 05/12/2005 by Merrick, Inc. The total survey area was around 1,190.00 km^2 with the point density of 1.41 points/m^2. The Horizontal and Vertical Coordinates reference is NAD83 California State Plane Zone VI FIPS 0406 Feet [EPSG: 2875] and NGVD29 Feet respectively.

2) Hyperspectral data: The hyperspectral data has been downloaded from AVIRIS data portal where it is freely available, URL: http://aviris.jpl.nasa.gov/alt_locator/. The airborne hyperspectral imagery was acquired on 16th November 2011 at the time 16:19:00 UTC. The hyperspectral sensor used was AVIRIS and the average altitude of the sensor above the ground was 20km. The imagery consisted of 224 bands in 365.93-2496.23 nm region. The spatial and spectral resolutions were 4.5m and 9.92nm, respectively. The spatial reference is UTM, Zone 11 North.

I. Methodology

A. *Data Preprocessing*

Preprocessing of Hyperspectral data was done to convert radiance data into reflectance data by applying sensor and atmospheric corrections. Sensor corrections include bad band removal i.e. all the noisy and zero value bands using ENVI software version 5.0. AVIRIS hyperspectral data consists of 224 bands out of which 44 bands were noisy. Hence after removal of bad bands the data only consisted of 180 bands. Table 1 shows all the bad bands.

Table.1 Bands with zero values or noise

Bad Bands
1, 2, 3, 4, 5, 107, 108, 109, 110, 111, 112, 113, 114, 115, 116, 152, 153, 154, 155, 156, 157, 158, 159, 160, 161, 162, 163, 164, 165, 166, 167, 168, 169, 170, 171, 172, 173, 174, 175, 176, 221, 222, 223, 224

After the removal of bad bands, atmospheric correction was performed in ENVI atmospheric correction module i.e. Fast Line-of-sight Atmospheric Analysis of Hypercube (FLAASH) based on MODTRAN. FLAASH correction is done to remove all the adverse effects of atmosphere and to determine true surface reflectance values [13]. There are certain area specific and data specific parameters which needs to be mentioned for applying atmospheric correction to a dataset. The input parameters used by the FLAASH atmospheric correction module are listed in Table 2.

Table.2 Input parameters used for the atmospheric correction of hyperspectral dataset

FLAASH parameters	**Value given for Hyperspectral data**
Scene Centre Latitude	32^o 41'
Scene Centre longitude	-117^o 6'
Scaling Factor	300 for band 6-110 & 600 for rest
Pixel Size	4.5 m
Sensor Type	Hyperspectral-AVIRIS
Flight Date	16th November 2011
Average Flight Time	19:16:00
Sensor Altitude	20 km
Ground Elevation	0.249
Atmospheric Model	U.S. Standard
Water Retrieval	No
Aerosol Model	Urban
Aerosol Retrieval	None
Initial visibility	40 km

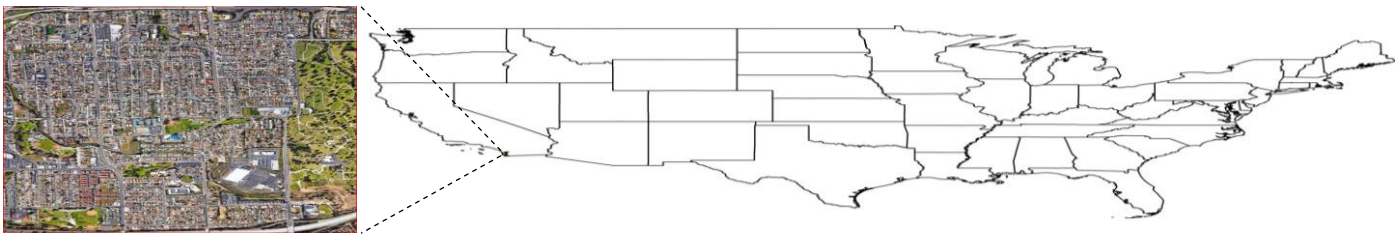

(a) (b)

Fig. 1. (a) Study Area (google earth) (b) Location of Study Area

B. Indices calculation & nDSM generation

Two indices were calculated in this study namely Normalized Difference Vegetation Index (NDVI) and Normalized Differential Built-up Index (NDBI). NDVI is a numerical indicator that uses the visible and near-infrared bands of the electromagnetic spectrum, and is adopted to analyze remote sensing measurements and assess whether the target being observed contains live green vegetation or not. NDVI was calculated from equation 1.

$$NDVI = \frac{NIR - Red}{NIR + Red} \quad (1)$$

Where NIR is the reflectance in Near Infra-Red Band and Red is the reflectance in Red band of the spectrum. NDBI is the numerical indicator that uses the short wave infra-red and near infra-red bands of electromagnetic spectrum for mapping built-up areas. NDBI is calculated from equation 2.

$$NDBI = \frac{SWIR - NIR}{SWIR + NIR} \quad (2)$$

Where NIR is the reflectance in Near Infra-Red Band and SWIR is the reflectance in Short wave infra-red band of the spectrum. Digital Surface Model (DSM) and Digital Elevation Model (DEM) generated using ENVI 5.0 software are of the resolution of 1 m. nDSM is generated by subtracting DEM from DSM by equation 3.

$$nDSM = DSM - DEM \quad (3)$$

The generated nDSM was then co-projected with the AVIRIS reflectance image using ERDAS 2014 software. The projected nDSM is of 4.5 m resolution as that of AVIRIS image.

C. Classification

1) Supervised classification: For the classification of Hyperspectral data a supervised classification technique Spectral Angel Mapper (SAM) has been used. SAM algorithm is based on an assumption that every single pixel of remote sensing image represents one certain ground cover material, thus can be uniquely assigned to only one ground cover class. The SAM algorithm determines the spectral similarity between two spectra by calculating the angle between the two, treating them as vectors with dimensionality equal to the number of bands [14]. In this algorithm the spectral similarity has been determined using equation 4

$$\alpha = \cos^{-1}\left(\frac{\sum_{i=1}^{nb} t_i r_i}{\sqrt{\sum_{i=1}^{nb} t_i^2}\sqrt{\sum_{i=1}^{nb} r_i^2}}\right) \quad (4)$$

Herein, *nb* is the number of bands in the image; *t* is pixel spectrum; *r* in reference spectrum and α is spectral angle.

The reference spectra for SAM classification was picked from ASTER spectral library. The ASTER spectral library includes data from three other spectral libraries: the Johns Hopkins University (JHU) Spectral Library the Jet Propulsion Laboratory (JPL) Spectral Library, and the United States Geological Survey (USGS - Reston) Spectral Library [15].

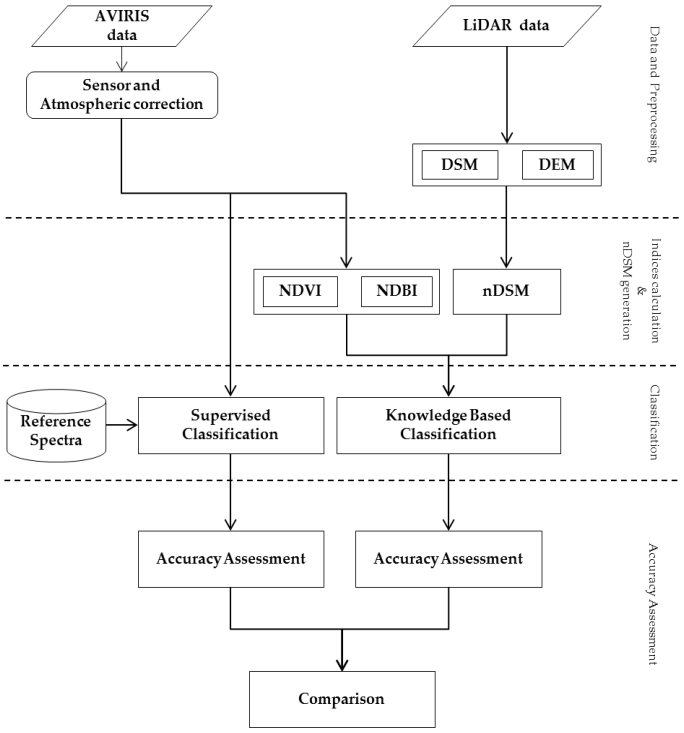

Fig. 2. Flowchart of methodology

For the calculation of spectral separability of these 8 classes spectral Analyst in ENVI 5.0 was used according to which variable angles for different classes in SAM classification were decided. The spectra from ASTER spectral library were also resampled to match with the 180 bands of AVIRIS data. Angles given to different classes for performing SAM classification is shown in Table 3.

Table 3. Angles given for SAM classification

Material	Angle used for SAM classification
Asphalt concrete road	0.2
Construction concrete	0.22
Paving asphalt road	0.25
Reddish asphalt shingle	0.2
Slate stone shingle	0.3

Vegetation Grass	0.35
Vegetation Tree	0.18
Gravelly sandy loam	0.22

2) Knowledge based classification: For the integration of Hyperspectral and LIDAR data, a knowledge based classification (KBC) was carried out. The variables used in Knowledge based classification are NDVI, NDBI which were derived from AVIRIS reflectance image and nDSM which has been derived from the point cloud LiDAR data. Knowledge based classification was done in ERDAS imagine 2014 software after doing the co-registration of all three. The set of hypothesis, rules and variables used is shown in Figure 3.

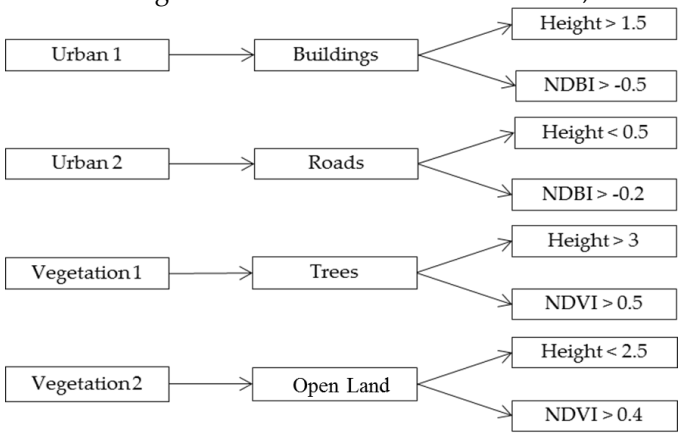

Fig. 3. Decision tree for knowledge based classification

D. Accuracy Assessment

The accuracy assessment of the thematic maps was based on the error matrix, which was calculated from ERDAS imagine 2014 [16].For this we compared certain randomly distributed pixels in the classified image to the reference pixels. There were 51 validation pixels taken, for which the classes were found out from the Hyperspectral image. As a result, overall accuracy (OA), producer's accuracy (PA) and kappa coefficient (κ) were calculated. The error matrix is an n * n matrix where rows representing classification samples and the columns representing the reference samples [17]. The kappa coefficient can be defined as a multivariable statistical method which is used for assessing classification accuracy and can be defined as in equation (5) [18].

$$\kappa = \frac{n\sum_{k=1}^{q} n_{kk} - \sum_{k=1}^{q} n_{k+}n_{+k}}{n^2 \sum_{n=1}^{q} n_{k+}n_{+k}} \quad (5)$$

Herein, κ is the kappa coefficient; q is the number of rows in the error matrix; n_{kk} is the observation in row k and column k; and n_{k+} and n_{+k} are the sums of all observations of row k and column k [18]. [19]

II. RESULTS AND DISCUSSIONS

A. Atmospheric Correction

FLAASH Atmospheric correction model is used for the correction of AVIRIS radiometric data. Results of the spectral profiles before and after atmospheric correction of the datasets were compared by observing spectra of building, road and vegetation and they have shown significant improvement in the spectral profile after atmospheric correction. The results obtained for the three features before and after atmospheric correction are explained in Figure 4 in terms of their spectral profiles.

It can be seen in the spectral signatures that all the water absorption bands have been removed from the spectral signatures. Spectra of grass shows reflectance at green band and very high reflectance at NIR band but not so obvious absorption in red band may be because of some processing errors. The building spectra which is most probably made of concrete has spectral signature very close to concrete. Almost all the spectra after atmospheric correction have higher reflectance than before.

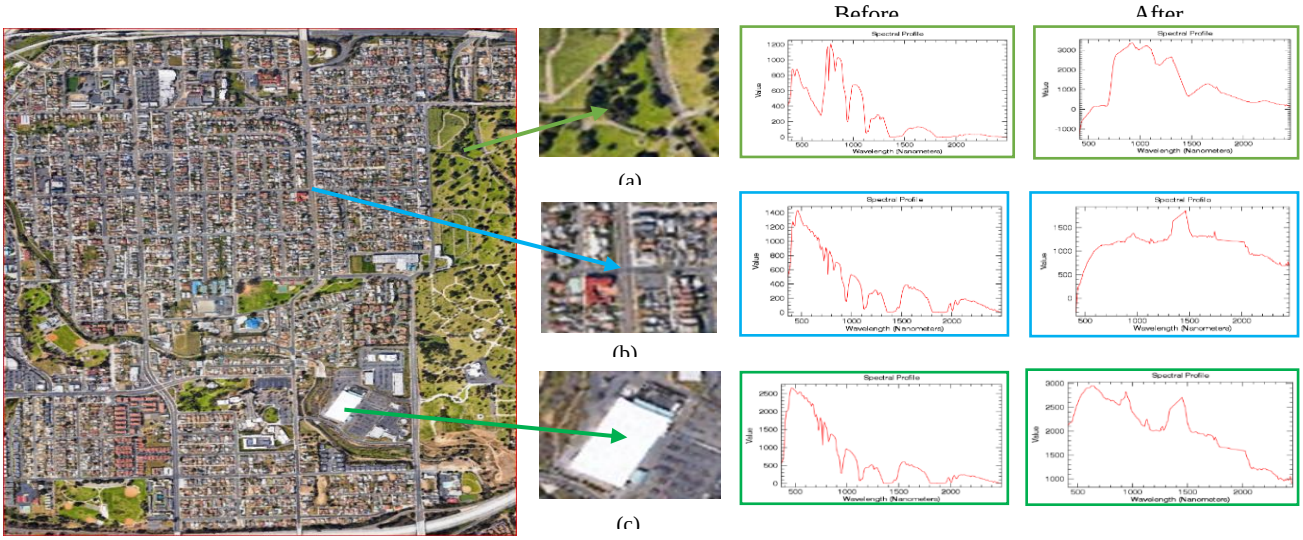

Fig. 4. (a) Vegetation, (b) Road and (c) Building spectra before and after atmospheric correction

B. Spectral Angle Mapper classification

Spectral Angle Mapper Classification approach is used for the Classification of Hyperspectral Data. The classes used were 8 with spectra derived from ASTER spectral library. As the main purpose of our study was to extract buildings, roads, trees and open land, so we merged these classes into 4 broader classes. The classification result after the merging of classes is shown in figure 5.

Fig. 5. SAM classified image

In this classified image it can be seen that at some points, buildings and roads are misclassified because of spectral similarity between the rooftop material and road material e.g. paving asphalt and reddish asphalt shingle. Even in the vegetation at some points are misclassified due to huge spectral similarity between grass and tree spectra. The overall accuracy of this SAM classified image was found to be 60.78%. Accuracy assessment of the classification results is shown in Table 4.

C. Normalized Digital surface Model

As stated earlier in the methodology nDSM is generated by subtracting DEM from DSM which were earlier derived from point cloud LiDAR data. The main purpose of calculation of nDSM is to get the height of manmade (buildings and roads) and natural (trees and grass) features above the surface of earth.

D. Normalized Differential Vegetation Index

NDVI was calculated from the hyperspectral data to get the greenness of study area. In the study area NDVI ranges from .4 to 1 for grass and .5 to 1 for tree. And for buildings and roads it is lesser than 0.2 but we have not taken NDVI into consideration for knowledge based classification.

E. Normalized Differential Built-up Index

NDBI is used to calculate density of Roads and buildings in the study area. It was found that for roads NDBI ranges from -0.2 to 1 while for the buildings it ranges from -0.5 to 1.

Table 4. Accuracy of individual classes

Classes	Accuracy (%)		Kappa Coefficient		Producer's Accuracy (%)	
	SAM	KBC	SAM	KBC	SAM	KBC
Unclassified	-	-	0.0000	0.0000	-	-
Buildings	33.33	73.33	0.2924	0.5879	65	61.11
Roads	62.9	100	0.9273	1.000	83.33	80
Trees	100	84.62	1.0000	0.7879	27.27	78.57
Grass	50	33.33	0.4446	0.2766	69.05	25

F. Knowledge based classification

For knowledge based classification the set of hypothesis, rules and variables are previously shown in methodology. Classified image according to those rule is shown in Figure 6. The accuracy of 68.63% was achieved for this classification. Accuracy assessment of the classification results is shown in Table 4.

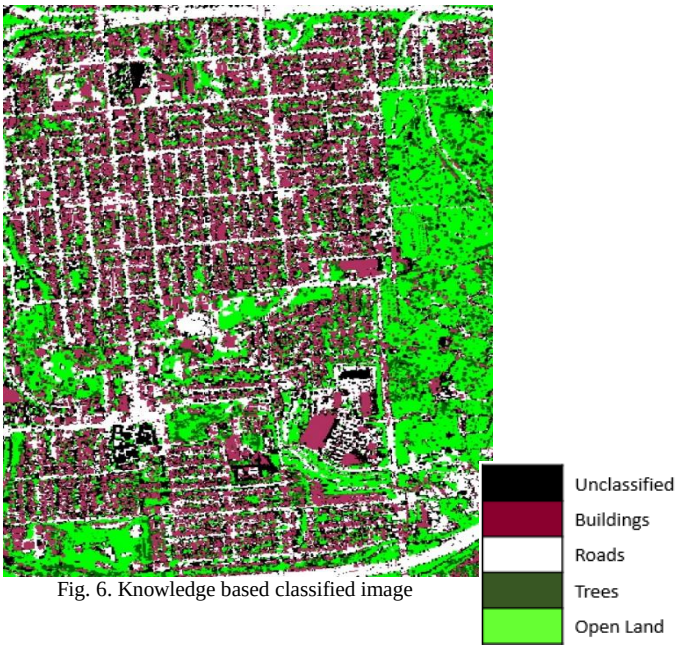

Fig. 6. Knowledge based classified image

G. Comparative analysis of accuracy

The accuracy achieved for knowledge based classified image was around 8% more than the SAM classified image which shows that the classification result of knowledge based classification was more accurate as compared to SAM classification. Some of the areas were chosen for comparison of results and the results are shown in figure 7.

In figure 7 (a), the SAM classified image the 'D' road is not classified properly while in the knowledge based classified image the classification is more precise. The 'D' shape of road is clearly seen in the knowledge based classified image. In figure 7 (b), the subset which is a building made of construction concrete has not been classified properly in SAM classification.

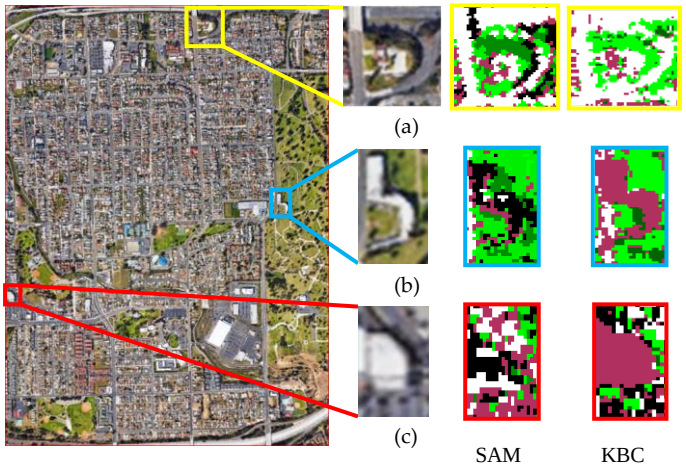

Fig. 7. Comparison between SAM and KBC classification

In SAM classified image most of the building is either unclassified or covered with paving asphalt road with a very little part of construction concrete. But as we analyze the knowledge based classified image the building boundary is clearly visible. In figure 7 (c), we can clearly visualize the increase in accuracy of knowledge based classified image in which the building boundary is clearly visible which is not at all visible in the SAM classified image.

III. CONCLUSION

The results of SAM experiments indicate that classification accuracy is not satisfactory in standard cases involving only Hyperspectral imagery. However, the incorporation of LiDAR data, especially NDSMs, significantly improves accuracy. Thus, urban classification is highly dependent on LiDAR height rather than on multispectral or Hyperspectral imagery.

Knowledge-based classification rules improved urban classification performance. Three factors may explain the success of this method. First, the four height-level classification framework not only reduces the number of categories at each level but also overcomes the ambiguity between high-height and low-height objects. In addition, the KBC successfully removes shadows between buildings from the preliminary classified image. The KBC experiment results indicate that the overall accuracy of the KBC is 8 percent better than that of the SAM approach. Moreover, the visual details in the KBC are superior to those of the SAM. .

The KBC provides the procedures and mechanisms to formalize knowledge into classification rules. The advantage of the KBC is that its procedure can be repeated by designing a stand-alone program or applying the rules to commercial classification software with "expert system" functionality, such as ERDAS Imagine®. In the future, more subcategories can be extended to the KBCS according to user requirements. More ground-feature discriminative models and inference rules can be explored if more subcategories are needed for enhanced accuracy results.

IV. REFERENCES

[1] R. L. Powell, D. A. Roberts, P. E. Dennison and L. L. Hess, "Sub-pixel mapping of urban land cover using multiple endmember spectral mixture analysis: Manaus, Brazil," Remote Sensing of Environment, vol. 106, p. 253–267, 2007.

[2] C. Small, "A global analysis of urban reflectance," International Journal of Remote Sensing, vol. 26, no. 4, p. 661–681, 20 February 2005.

[3] C. Small, "Estimation of urban vegetation abundance by spectral mixture analysis," International Journal of Remote Sensing, vol. 22, no. 7, pp. 1305-1334, 2001.

[4] W. B. Clapham, "Continuum-based classification of remotely sensed imagery to describe urban sprawl on a watershed scale," Remote Sensing of Environment, vol. 86, p. 322–340, 2003.

[5] M. Ji and J. R. Jensen, "Effectiveness of Subpixel Analysis in Detecting and," Geocarto International, vol. 14, no. 4, pp. 33-41, December 1999.

[6] R. Pu, P. Gong and R. Michishita, "Spectral Mixture Analysis for mapping of abundance of Urban Surface Components from the Terra/ASTER data," in ASPRS, Tampa, Florida, 2007.

[7] W. Xu. M. Wooster and C. Grimmond, "Modelling of urban sensible heat flux at multiple spatial scales: A demonstration using airborne hyperspectral imagery of Shanghai and a temperature–emissivity separation approach," Remote Sensing of Environment, vol. 112, p. 3493–3510, 2008.

[8] S. Li, H. Wu, D. Wan and J. Zhu, "An effective feature selection method for hyperspectral image classification based on genetic algorithm and support vector machine," Knowledge-Based Systems, vol. 24, no. 1, p. 40–48, February 2011.

[9] M. Herold, D. A. Roberts, M. E. Gardne and P. E. Dennison, "Spectrometry for urban area remote sensing—Development and analysis of a spectral library from 350 to

2400 nm," Remote Sensing of Environment, vol. 91, p. 304–319, 2004.

[10] W. Zhou, "An Object-Based Approach for Urban Land Cover Classification: Integrating LiDAR Height and Intensity Data," IEEE Geoscience and Remote Sensing Letters, vol. 10, no. 2, pp. 928-931, July 2013.

[11] B. Abbasi, H. Arefi, B. Bigdeli, M. Motagh and S. Roessner, "Fusion of Hyperspectral and LIDAR data based on dimension reduction and maximum likelihood," in The International archives of the photogrammetry, remote sensing and spatial information sciences, Berlin, Germany, 2015.

[12] S. Luo, C. Wang, X. Xi, H. Zeng, D. Li, S. Xia and P. Wang, "Fusion of Airborne Discrete-Return LiDAR and Hyperspectral Data for Land Cover Classification," Remote Sensing, vol. 8, no. 1, 2016.

[13] D. G. Hadjimitsis, G. Papadavid, A. Agapiou, K. Themistocleous, M. G. Hadjimitsis, A. Retalis, S. Michaelides, N. Chrysoulakis, L. Toulios and C. R. I. Clayton, "Atmospheric correction for satellite remotely sensed data intended for agricultural applications: impact on vegetation indices," Natural Hazards and Earth Sciences, vol. 10, p. 89–95, 2010.

[14] Rashmi S, S. Addamani, V. and R. S, "Spectral Angle Mapper Algorithm for Remote Sensing Image Classification," International Journal of Innovative Science, Engineering & Technology, vol. 1, no. 4, June 2014.

[15] A. M. Baldridge, S. J. Hook, C. I. Grove and G. Rivera, "The ASTER spectral library version 2.0," Remote Sensing of Environment, vol. 113, p. 711–715, 2009.

[16] R. G. Congalton, "A review of assessing the accuracy of classifications of remotely sensed data," Remote Sensing of Environment, vol. 37, no. 1, pp. 35-46, July 1991.

[17] S. V. Stehman, "Selecting and interpreting measures of thematic classification accuracy," Remote Sensing of Environment, vol. 62, no. 1, pp. 77-89, October 1997.

[18] G. M. F. M. Foody, "Status of land cover classification accuracy assessment," Remote Sensing of Environment, vol. 80, p. 185 – 201, 2002.

[19] G. P. Petropoulos, K. Arvanitis and N. Sigri, "Hyperion hyperspectral imagery analysis combined with machine learning classifiers for land use/cover mapping," Expert systems with Applications, vol. 39, no. 3, pp. 3800-3809, 15 2 2012.

[20] M. Ruijin, "Rational Function Model in Processing Historical Aerial Photographs," Photogrammetric Engineering & Remote Sensing, vol. 4, no. 9, pp. 337-345, April 2013.

[21] C. Pohl and J. L. Van Genderen, "Review article Multisensor image fusion in remote sensing: Concepts, methods and applications," International Journal of Remote Sensing, vol. 19, no. 5, p. 823±854, 1998.

[22] J. E. Mesina, "Urban Classification Techniques Using the Fusion of LiDAR and Spectral Data," Monterey, California, 2012.

[23] Q. Man, P. Dong and H. Guo, "Pixel- and feature-level fusion of hyperspectral and lidar data for urban land-use classification," International Journal of Remote Sensing, vol. 36, no. 6, pp. 1618-1644, 2015.

[24] M. Herald and D. A. Robert, "Multispectral Satellites- Imaging Spectrometry- LIDAR: Spatial- spectral tradeoffs in urban mapping," International journal of Geoinformatics, vol. 2, no. 1, pp. 1-13, March 2006.

[25] L. Hashemi Beni, S. McArdle and Y. Khayer, "An Integrated Method For Mapping Impervious And Pervious Areas In Urban Environments Using Hyperspectral And Lidar Data," in ISPRS Annals of the Photogrammetry, Remote Sensing and Spatial Information Sciences, Toronto, Canada, 2014.

[26] A. Elaksher, "Fusion of Hyperspectral images and LIDAR based DEMs for coastal mapping," in The International Archives of the Photogrammetry, Remote sensing and spatial information sciences, Beijing, 2008.

[27] C. Debes, J. Hahn, W. Liao, S. Gautama and Q. Du, "Hyperspectral and LiDAR Data Fusion: Outcome," IEEE Journal Of Selected Topics In Applied Earth Observations And Remote Sensing, vol. 7, no. 6, June 2014.

[28] C. Debes, A. Merentitis, R. Heremans, J. Hahn, N. Frangiadakis and T. v. Kasteren, "A two-stream frame work for LiDAR and Hyperspectral Imagery," Darmstadt, Germany, 2013.

[29] J. C. Giarratano and Riley, "Expert Systems," PWS Publishing Co, 1998.

[30] M.-J. Huang, S.-W. Shyue and L.-H. Lee, "A Knowledge-based Approach to Urban Feature Classification Using Aerial Imagery with Lidar Data," Photogrammetric Engineering & Remote Sensing, vol. 74, no. 12, p. 1473–1485, December 2008.

[31] S. A. Rahman, W. A. Aliady and N. I. Alrashed, "Supervised Classification Approaches to Analyze Hyperspectral data," I.J. Image, Graphics and Signal Processing, vol. 5, pp. 42-48, 2015